Journal of Loss Prevention in the Process Industries 102 (2026) 105999

Contents lists available at ScienceDirect

Journal of Loss Prevention in the Process Industries

journal homepage: www.elsevier.com/locate/jlp

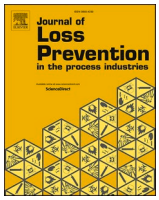

Influence of different storage tank bunding configurations on the dispersion of flammable vapour cloud generated by an overfilling incident

Fabrizio Santamato [1], Carmelo Sofia [1], Valentina Busini [*]

Chemical, Materials and Chemical Engineering "G. Natta" Department, Politecnico di Milano, Italy

ARTICLE INFO

Keywords:
Fire mitigation
Bund design
CFD
Mitigation barriers
Buncefield
Overfilling

ABSTRACT

The high risk associated with storage tanks is due to the high volumes of substances stored and their hazardous characteristics. Loss of containment events may result in severe consequences. For this reason the implementation of effective protective measures, such as bunding systems, are essential to mitigate potential damage.

This work investigates how different bund configurations affect the dispersion of a flammable vapour cloud generated by a tank overfilling scenario. The analysis was performed using computational fluid dynamics (CFD), considering an overfilling event similar to the 2005 Buncefield accident. Unlike previous studies, both cascade and pool evaporation were modelled simultaneously using a wall-film approach. Results show that neglecting pool evaporation significantly underestimates vapour generation, with evaporated mass increasing from 11.8% to 66.6% when the pool contribution is included.

An extensive parametric study of bund configurations was conducted varying the tank–wall distance, bund wall height, number of tanks, basin burial, anti-overtopping deflectors, and wind direction.

Bund geometry was found to significantly affect both source term and damage distances. Increasing the bund wall height from 1.8 m to 3.6 m reduces LFL/2 damage distances by about 45%. Conversely, complete burial of the basin may increase damage distances by up to 9% due to reduced turbulence and mixing. Anti-overtopping deflectors reduce damage distances by roughly 20%, while frontal wind conditions increase them by more than 20%.

1. Introduction

Global demand for petroleum products, used both as energy carriers and as feedstocks for downstream processing, remains significant despite the progressive introduction of alternative energy technologies. The production and distribution chain requires the storage of large quantities of hazardous substances whose accidental release, due to their flammability and toxicity, may result in severe consequences for human health and the environment, both within and beyond plant boundaries. In many cases, the inventories involved are such that these facilities fall under the scope of Directive 2012/18/EU (Seveso III), which regulates establishments handling dangerous substances with major accident potential.

Mapping analyses of major accident hazard establishments show that such facilities are widely distributed across Europe. For logistical and distribution reasons, storage depots are often located in strategically accessible yet highly vulnerable areas, including industrial ports and densely populated urban regions. This geographical distribution further amplifies the potential societal risk associated with large storage installations.

These considerations underline the importance of comprehensive risk assessment, as well as the identification of effective preventive and protective measures aimed at reducing both the frequency and severity of potential accidents. This aspect is particularly relevant for storage-related incidents, which are typically characterized by low probability but high consequence.

Among the main protective measures adopted for storage tanks is the construction of containment dikes (bunds), primarily designed to physically retain spilled liquid within the basin in the event of loss of containment (API 650; BS 2654). While their fundamental function is to prevent liquid spread and potential domino effects within the facility, bunds may also provide an additional safety benefit. By acting as passive barriers, they can partially confine the flammable vapour cloud generated by an accidental release, limiting its dispersion into the

* Corresponding author.
E-mail address: valentina.busini@polimi.it (V. Busini).
[1] Shared co-first authorship.

https://doi.org/10.1016/j.jlp.2026.105999
Received 8 January 2026; Received in revised form 16 March 2026; Accepted 16 March 2026
Available online 19 March 2026

surrounding environment and retaining it, as far as possible, within areas where ignition sources are controlled or excluded (API 2350; HSG176).

Storage tanks may experience various failure modes, ranging from small shell leaks to catastrophic rupture. A comprehensive risk analysis requires the preliminary assessment of all credible scenarios before identifying the worst cases for detailed investigation. Among these scenarios, overfilling represents one of the most critical. Unlike instantaneous catastrophic failures, the discharge rate during an overfilling event is governed by the feed pump capacity and may persist for an extended period. Consequently, the total released mass can exceed the nominal tank volume. Moreover, overfilling often generates a free-falling liquid cascade from the tank roof, whose evaporative contribution adds to that of the liquid pool forming on the bund floor.

Historical analyses of storage tank incidents between 1960 and 2003 (Chang and Lin, 2006) identified overfilling as the most frequent operational failure mode, leading to fire or explosion in 86.7% of cases. A further review of open-access accident databases covering the period from 2003 to the present indicates that this trend has not significantly declined. Even after the 2005 Buncefield accident, widely regarded as a turning point in awareness of overfilling hazards, additional major incidents have occurred, including the 2009 Puerto Rico explosion.

The 2005 Buncefield accident involved a massive explosion and prolonged fire at an oil storage depot in Hertfordshire, United Kingdom, triggered by the overfilling of a gasoline tank. It was one of the largest peacetime explosions in Europe, causing extensive structural damage and widespread environmental contamination. Although no fatalities occurred, more than 40 people were injured, and 23 storage tanks were affected during a fire that lasted five days.

Analysis of past accident data shows that, in overfilling events involving flammable liquids, ignition is usually unavoidable once a sufficiently large vapour cloud forms. Eliminating ignition sources within the storage area is necessary but not sufficient, as the vapour cloud may extend well beyond the facility boundary into areas where ignition control cannot be guaranteed (Chang and Lin, 2006). Under such conditions, ignition can trigger severe domino effects involving multiple tanks and process units both within and outside the installation.

Recent studies have also focused on the prevention of tank overfilling through structured risk assessment methodologies. For instance, a recent work applying Layers of Protection Analysis (LOPA) to storage tank overfilling scenarios highlighted the effectiveness of multiple independent protection layers in reducing failure probability and associated risk (Sotoodeh, 2024).

Previous studies have investigated the influence of bund geometry on accident consequences in storage tank facilities. A related study was presented by Zhao et al. (2022), who investigated the capability of different bund configurations to retain the released liquid and prevent overtopping outside the containment area. In that work, a reduced-scale experimental campaign was conducted in which model tanks, partially filled with water as a surrogate for LNG, have been subjected to controlled agitation to quantify the fraction of liquid escaping the containment basin.

The same scenario was investigated by Luan et al. (2023) by developing a multiphase CFD model to simulate LNG overtopping events, including liquid release, spreading, evaporation, and vapour dispersion. Despite some similarities in the aim of the study and the modelling approach, important differences exist with the present work. In LNG releases from cryogenic storage systems, evaporation is largely governed by heat transfer processes, whereas the evaporation of n-hexane, used in the present study as a surrogate for gasoline released from atmospheric storage tanks, is mainly driven by mass transfer mechanisms.

To assess the accident scenario generated by a storage tank, it is necessary to refer to the specific tank typology considered. Historical analyses analysis (Chang and Lin, 2006; Persson and Lönnermark, 2004) indicate that gasoline has been the substance most frequently involved in high-consequence storage tank accidents in recent decades. Due to its physicochemical properties, namely being a volatile organic compound (VOC), subcooled under storage conditions, and highly flammable, it is typically stored in external atmospheric tanks equipped with either a floating roof or a fixed roof with an internal floating deck and Pressure–Vacuum Valves (PVVs) (API 650).

With reference to fixed-roof tanks with internal floating decks, the same typology involved in the Buncefield accident, the most credible release scenario identified in the literature involves failure along a portion of the tank circumference. PVVs are installed to prevent excessive internal pressure variations and the formation of explosive atmospheres in the vapour space. They are designed to allow the passage of air and vapours in and out of the tank, thereby maintaining the internal pressure approximately equal to atmospheric pressure under both filling and emptying conditions (Atkinson et al., 2015; Atkinson and Gant, 2012a).

During an overfilling incident, if dedicated safety systems for diversion or shut-off are absent or malfunctioning, the liquid may rise above the floating deck, pass the rim seals, and accumulate beneath the conical roof. Once the roof volume is filled, the liquid may reach the PVVs located at the top of the tank. Since these devices are designed for vapour flow rather than liquid discharge and have limited flow area, internal pressure may increase significantly. The resulting overpressure can lead either to the ejection of a pressurized liquid spray through the valve or, more plausibly, to structural failure of the tank, which is not designed to withstand internal liquid overpressure. According to API 650, structural rupture is most likely to occur at the shell-to-roof weld. This configuration, commonly referred to as a “frangible roof,” is intended to protect the shell-to-bottom joint in the event of internal overpressure caused by external fire exposure. It is not specifically designed as a protective measure against overpressure resulting from overfilling. Therefore, the scenario described here represents a conservative but credible limit case, consistent with historical evidence, in which all preventive measures associated with overfilling have failed.

The generation of flammable vapours during an overfilling event involves multiple interacting physical processes. Experimental investigations (Atkinson and Coldrick, 2012; Coldrick et al., 2010, 2011) have examined the liquid cascade component of such releases, although these studies were limited in geometric scale and duration. Experiments conducted with water and n-hexane as test fluids showed that releases similar to the Buncefield event produce droplets with average diameters on the order of 2 mm and temperatures at the base of the cascade ranging between −3.6 °C and −6.3 °C (Coldrick et al., 2011).

Complementary computational fluid dynamics (CFD) studies (Atkinson et al., 2015; Atkinson and Coldrick, 2012) have been carried out to model vapour cloud generation and characterize its main parameters. In particular, CFD models of the liquid cascade were developed and validated against the aforementioned experimental data. These studies demonstrated that the liquid cascade stabilizes approximately 20 s after the onset of release for geometries comparable to those observed in the Buncefield accident (Atkinson and Gant, 2012a).

Following the release, the resulting liquid pool is subject to simultaneous heat and mass transfer processes. In fire scenarios involving the storage tank, thermal radiation becomes the dominant mechanism driving evaporation. The evaporation rate of petroleum products under fire exposure has been assessed in the literature (Ginestet and Le Bot, 2018), often approximating the hydrocarbon mixture as pure n-hexane. The adoption of n-hexane or n-heptane as representative surrogates for light petroleum fractions is a common simplification in the scientific literature (Huang et al., 2020a, 2020b; Wang et al., 2022), as it provides a reasonable approximation of the thermophysical behaviour of gasoline-type products.

In cases of delayed ignition, the vapour cloud generated by pool evaporation disperses under the influence of ambient wind and atmospheric stability conditions. This dispersion process can be investigated using different modelling approaches.

Classical theoretical models for vapour cloud dispersion (e.g., integral and Gaussian-type models) are widely used in quantitative risk assessment due to their limited computational cost, they are generally based on simplified geometrical assumptions and homogeneous flow fields. However, such models typically cannot account explicitly for the presence of complex obstacles, large containment basins, multiple tanks, or for the coupled interaction between pool evaporation, cascade evaporation and local turbulence induced by bund walls.

The CFD approach, which is the one adopted in this work, provides detailed information on the local flow field, turbulence distribution and concentration gradients, allowing the identification of the physical mechanisms responsible for changes in source term and damage distances. In particular, the simulations highlight how bund wall height, deflectors, tank wake effects and basin burial modify air entrainment and mixing processes, which are not directly represented in classical models.

Several CFD studies have investigated the dispersion of flammable vapour clouds in the presence of containment dikes, generally neglecting the formation and evaporation of liquid pools (Atkinson et al., 2008, 2015; Cheng et al., 2026; Coldrick et al., 2011; Gant and Atkinson, 2011). In such scenarios, bund walls act as physical obstacles that influence both the direction of cloud propagation and its geometric development. Their configuration may also alter the local flow field within and around the basin, thereby affecting air entrainment (i.e., dilution) and, consequently, the spatial extent of hazardous concentrations.

The influence of fixed obstacles on dense gas dispersion has been widely examined using CFD approaches ((Busini et al., 2012); Busini and Rota, 2014; Derudi et al., 2014; Marsegan et al., 2016), providing valuable insights for dike design. These studies indicate that increasing barrier height enhances mitigation efficiency, whereas increasing wall roughness has negligible influence on the downwind distance at which the lower flammability limit (LFL) is reached, due to its limited impact on turbulence generation. Furthermore, it has been shown that small geometric modifications aimed at locally increasing turbulence are generally ineffective, as the inertia of dense clouds prevents significant alteration by small-scale obstructions (Busini and Rota, 2014). In contrast, flow deflection strategies and active barriers have demonstrated greater mitigation potential (Busini and Rota, 2014; Marsegan et al., 2016).

In the present work, CFD models were employed to evaluate the effectiveness of containment dikes in reducing the damage area associated with a gasoline overfilling scenario in an atmospheric storage tank. The analysis focused on the influence of characteristic basin dimensions and configurations on vapour cloud dispersion and containment performance.

As an innovation with respect to the existing literature, the present work considers not only droplet evaporation from the liquid cascade, for which “escape” condition is adopted in the models, but also the formation and evaporation of the liquid pool in the absence of flame, through the implementation of a “wall-film” model. Despite wall-film modelling is a well-established CFD approach for representing liquid accumulation and evaporation, its quantitative impact on consequence assessment in tank overfilling accident chains has not been systematically evaluated. One of the core contributions of this study is therefore the demonstration of how the transition from a cascade-only representation to a combined cascade + pool evaporation model significantly alters the predicted source term and, consequently, the evaluated effectiveness of different bund configurations.

By explicitly quantifying these differences, the study provides engineering insight into the potential consequences of simplified source-term assumptions, which may otherwise lead to non-conservative or misleading conclusions in containment design and consequence analysis.

Initially, vapour generation from the liquid cascade alone was simulated to ensure comparability with previous CFD studies and to allow validation against available experimental data. Sensitivity analyses were subsequently conducted on selected modelling parameters (e.g., wall boundary conditions) to establish a robust reference model for the parametric investigation of bund configurations.

The influence of basin geometry was then examined by varying wall height and basin surface area, as well as by analysing alternative configurations, including the presence of a second tank within the same basin, complete burial of the basin below ground level, and the installation of deflectors designed to mitigate overtopping. Overtopping refers to the overflow of liquid beyond the basin boundaries due to the dynamic wave generated during an accidental release. This phenomenon has been frequently reported in past storage tank accidents, particularly in cases involving catastrophic bottom rupture. It has been extensively studied both experimentally (Atherton, 2005) and through mathematical modelling (Nair, 2008), and established correlations for estimating the fraction of liquid escaping the basin were adopted in the present analysis.

Finally, the influence of wind direction relative to the release location was assessed. For each configuration, both the source term and the resulting damage distances were evaluated.

The overall objective was to identify configurations that maximize containment efficiency and enhance vapour dilution through favourable airflow modification, thereby reducing the likelihood of ignition following release.

The Methodological Workflow of the Study is reported in Fig. 1.

2. Materials and methods

The simulations were carried out using the ANSYS Fluent software version 15(ANSYS, 2013).

The investigated accident scenario consists of the release of liquid to the atmosphere from the upper portion of an atmospheric storage tank located within a containment basin. In line with previous studies (Coldrick et al., 2010), the mathematical formulation accounts for droplet evaporation and the associated heat transfer processes, while other phenomena, such as droplet–droplet collisions and primary or secondary breakup, were neglected in a first approximation. Accordingly, the energy equation and species transport equations were activated.

Turbulence was modelled using the standard k–ε model, which remains one of the most widely adopted approaches in atmospheric dispersion studies and has been extensively validated in similar applications (Derudi et al., 2014; Luketa-Hanlin et al., 2007). All simulations were performed under neutral atmospheric stability conditions, with a reference wind speed of 5 m s^{-1}. The vertical wind profile was defined according to Monin–Obukhov similarity theory and implemented through a dedicated user-defined function.

To simplify the modelling of the multi-component condensed-phase hydrocarbon mixture (gasoline), the liquid was approximated as pure n-hexane, a surrogate commonly adopted in the literature that provides a reasonable representation of light petroleum fractions (Atkinson et al., 2015); this choice also ensures consistency with the validation study adopted in this work and, given that n-hexane is among the lighter and more abundant constituents within the gasoline boiling range, represents a reasonable and conservative single-component approximation for evaporation-driven dispersion analyses. The release was modelled as a spray of droplets with uniform initial diameter and temperature, neglecting the phenomenon of the break-up of the liquid stream into drops and filaments, in accordance with previous studies (Atkinson and Gant, 2012a). The initial droplet diameter was set to 2 mm, consistent with the experimental and numerical investigations reported by Atkinson et al. (2015), which were also used for the model validation.

In fact, the available break-up models, besides being very expensive in terms of computational costs, have been primarily developed to model the break-up of a liquid beam spilling from devices such as pressurized fuel injection systems (Atkinson et al., 2015; Coldrick et al.,

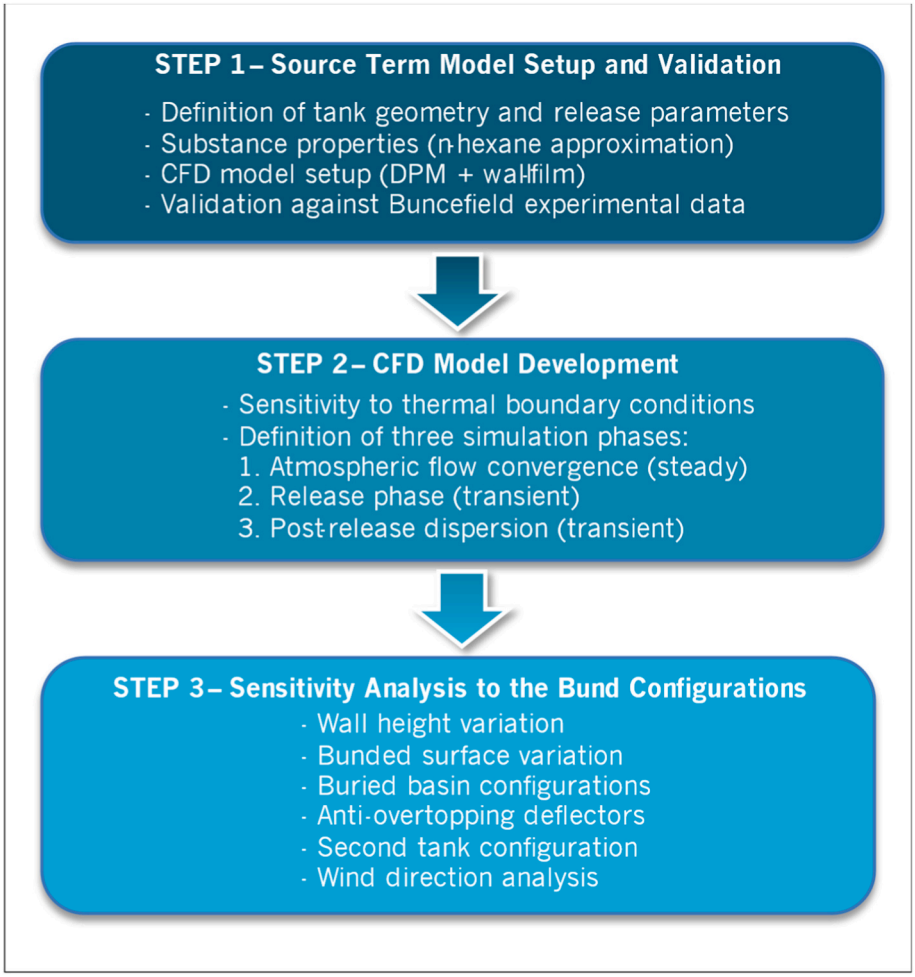

Fig. 1. Methodological workflow of the study.

2010), which differ significantly from overfilling conditions. Given the lack of information about their reliability in similar situations, and in agreement with existing literature, breakup phenomena were not considered.

A sensitivity analysis was performed to assess the influence of the splash parameter on the overall evaporation process. The results indicated that neglecting splash effects produces variations in the total evaporated mass of approximately 8%. Since the exclusion of splash slightly increases the predicted evaporated fraction, the adopted modelling choice can be considered conservative from a safety assessment perspective.

For the sake of conciseness, the detailed analysis and discussion of the splash sensitivity study are reported in the Supplementary Material, where the modelling assumptions and their quantitative impact are comprehensively documented.

The liquid release and subsequent droplet transport were simulated using the Discrete Phase Model (DPM), consistent with previous investigations (Atkinson and Gant, 2012a; Coldrick et al., 2011). Two alternative wall boundary treatments were considered, “escape” and “wall-film”, depending on the simulation objective.

3. Geometry, mesh and validation case

Given the complexity of the physical–chemical processes and structural configurations involved in a real overfilling accident, a number of modelling assumptions were introduced to ensure reliable simulations while maintaining acceptable computational costs. These simplifications, concerning both the mathematical representation of the accident scenario and the reproduced geometry, are consistent with approaches previously adopted in the literature (Atkinson and Coldrick, 2012; Atkinson and Gant, 2012b; Coldrick et al., 2010, 2011).

To simplify the geometrical representation, only the tank–basin system was included in the computational domain, neglecting accessory equipment and associated piping. The domain dimensions were selected to allow full development of the inlet wind profile before interaction with obstacles, in accordance with established guidelines for CFD simulations involving built structures and obstacles (Franke et al., 2011).

To reduce the number of total cells, thus optimizing computational efficiency, a locally refined subdomain was generated around the tank–basin system, ensuring higher mesh resolution in the region of interest. The domain was extended preferentially in the downstream wind direction, where the vapour cloud is expected to propagate (see Figure Fig. 2). To further narrow the grid around the bund walls, additional mesh refinement was introduced near the bund walls through the implementation of boundary layer elements to accurately capture near-wall flow and evaporation phenomena.

As a result of this domain configuration, the vapour cloud remains entirely within the computational domain throughout the simulations, and its dispersion profile develops fully without being affected by boundary truncation effects.

The release surface was modelled as an opening located at the top of the tank shell and extending over a portion of the tank circumference, as illustrated in Fig. 3. The dimensions of this surface were derived from reported mass flow rate and discharge velocity data, using the density of n-hexane (see Table 1). Assuming a discharge section covering 1/3 of the tank circumference and applying Bernoulli's equation with the specified

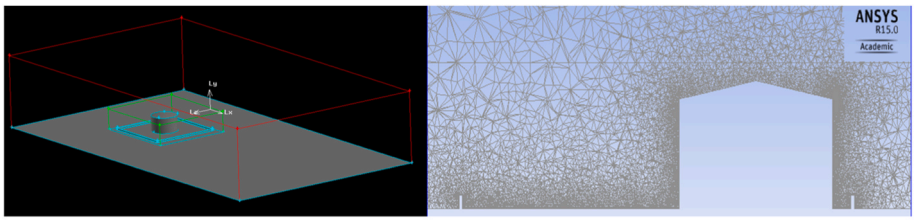

Fig. 2. Domain geometry in the Gambit software (a) and Characteristic of the grid in the Ansys Fluent software (b).

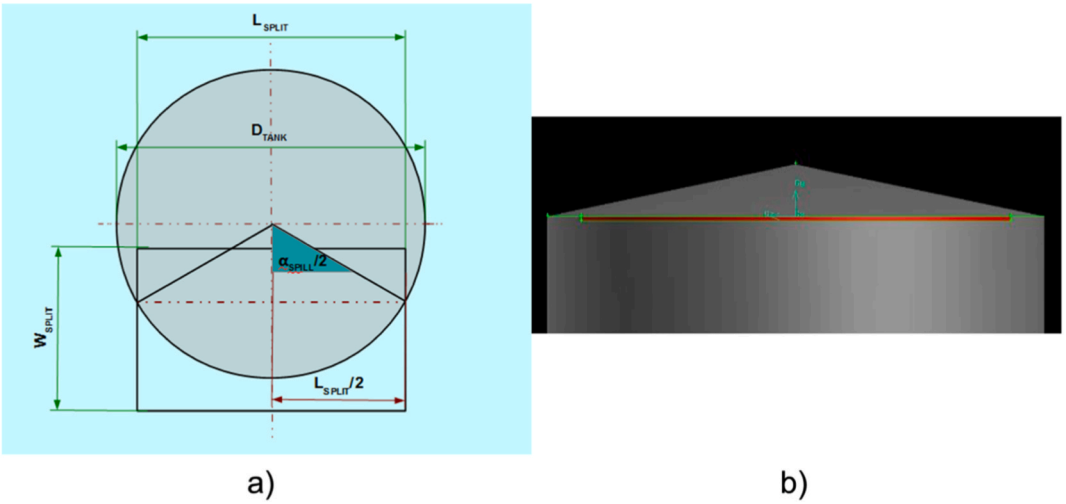

Fig. 3. Release geometry: Geometric representation (a), 3D view (b).

discharge velocity (equal to the initial horizontal droplet velocity), the resulting release area was estimated to be 0.16 m^2.

All containment basins considered in the study were modelled with a square plan geometry and a wall thickness of 0.6 m. Wall height and configuration were varied systematically to investigate their influence on vapour dispersion and damage distances.

The geometry and mesh were generated using Gambit software. Details of the mesh structure and the grid independence study are provided in the Supplementary Material.

For the overfilling scenario, the release rate was assumed equal to the maximum flow rate of the feed pump. The release duration was set to 20 s, corresponding to the minimum intervention time prescribed by Italian regulations for tanks equipped with automatic detection and shut-off systems (DM 15/5/96). This time interval is also consistent with previous CFD studies (Atkinson and Gant, 2012a), which demonstrated that the liquid cascade reaches quasi-steady stabilization within approximately 20 s.

Based on the considerations made, Table 1 summarizes the main characteristics of the CFD model used for the validation case.

Model validation was performed by comparing the results of the initial simulation with those reported for the Buncefield accident scenario (Atkinson and Gant, 2012a). In both studies, the droplet temperature decreases significantly due to latent heat loss associated with evaporation, reaching comparable values near the ground. Fig. 4(a) and (b) show, respectively, the droplet temperature distribution reported in the reference study and that predicted in the present work. The agreement between the two models is satisfactory and consistent with the experimental measurements reported by Coldrick et al. (2011), where droplet temperatures near the base of the cascade ranged between −3.6 °C and −6.3 °C.

Following validation against available experimental and numerical data, the model was employed for the parametric analyses described in the Results section.

4. Results

4.1. Analysis of the influence of evaporative contribution related to the pool

In previous CFD studies, the boundary condition typically adopted for the Discrete Phase Model (DPM) on solid walls is "*escape*" (Atkinson et al., 2015; Coldrick et al., 2010). Under this assumption, droplets crossing a solid surface leave the computational domain without interaction, and no liquid accumulation or pool formation is considered. However, a more realistic representation of an overfilling scenario assumes that once the liquid reaches the ground, it accumulates within the containment basin, forming a pool. Neglecting evaporation from this pool may lead to a significant underestimation of vapour generation and, consequently, of the associated hazard. For this reason, as a first step of the present analysis, the combined evaporative contributions of both the liquid cascade and the liquid pool were investigated.

For this purpose, the DPM framework was retained, modifying only the wall boundary condition from "*escape*" to "*wall-film*" to account for liquid accumulation and subsequent evaporation (i.e., ground surface and all the walls of the bund were defined as *wall-film* boundaries). With the wall-film approach, droplets impacting the basin floor contribute to the formation of a liquid film that evolves and evaporates over time, providing an additional source of vapour (see Table 2). In the Supplementary Materials a section provides a more detailed description of the wall-film model and how Fluent defines and computes the evaporative mass flow rate from the film. Table S7 summarizes all the boundary conditions adopted in the simulations.

Two main performance indicators were used to compare the analysed cases: (i) the vapour source term, expressed as the total percentage

Table 1
Main characteristics of the validation case and boundary conditions settings.

Characterization of the storage tank	Diameter	25 [m]
	Height	15 [m]
	Conic roof height	2.5 [m]
	Tank shell temperature	288.15 [K]
Characterization of the release	Release model	Spray DPM (Discrete Phase Model)
	Type of particle	Droplet
	Substance of the particle	n-hexane
	Drops initial diameter	2 [mm]
	Drops initial temperature	288.15 [K]
	Initial horizontal speed	1 [m/s]
	Release rate	105 [kg/s]
	Release duration	20 [s]
	Release elevation	12.5 [m]
	Release surface extension	1/3 D_{TANK} = 26.17 [m]
	Release surface height	6.1 [mm]
	Release surface	0.16 [m^2]
Characterization of the material	Ambient density	660 [kg/m3]
	Heat capacity	2512 [J/kg/K]
	thermal conductivity	0.137 [W/m/K]
	viscosity	0.00032 [kg/m/s]
	latent heat	336970 [J/kg]
Boundary conditions	Boundary condition for walls	Escape[a]
	Wind inlet, sky, lateral walls of the domain (5D)	Velocity inlet
	Wind outlet	Pressure outlet
	Wall temperature	273.15 [K]
	Wall roughness	0.01 m for concrete 0.0001 m for tank
	Thermal Boundary-Condition of the Soil and Basin	Isothermal[b]
	TSOIL = TBUND, [K]	= TAIR = 273.15
	Volume mixing law	Ideal gas

[a] The "escape" boundary condition applies only to the validation simulations performed against Atkinson et al. (2015), which is supported by experimental data and in which the same boundary condition was adopted. For the subsequent simulations, carried out to investigate the influence of different bund configurations, a "wall-film" boundary condition was selected.

[b] the "isothermal" boundary condition applies to all the simulations in the study, as the sensitivity analysis to the thermal boundary condition, performed in Section 4.2, showed a very limited differences between isothermal and adiabatic wall conditions.

of released substance that evaporates ($M_{EVAP\%}$), and (ii) the extent of the damage area. The latter was evaluated through the distances at which the concentration reaches half of the Lower Flammability Limit (½ LFL). According to Italian regulations (DM 15/5/96 and DM 20/10/98), this threshold defines the external boundary of the damage zone beyond which no severe effects are expected and corresponds to the lethality limit in the case of flash fire.

The characteristic distances considered in the analysis are illustrated and defined in Fig. 5.

Table 2 reports the results of the two simulations differing only in the DPM wall boundary condition ("*escape*" vs. "*wall-film*"). In both cases, the thermal boundary condition at the walls was set to "*isothermal*"; the influence of this assumption is addressed in the subsequent sensitivity analysis.

In the present study, all the quantitative results reported in the tables and concentration contour plots refer to simulation time t = 40 s. This instant includes 20 s of active release followed by 20 s of post-release dispersion. This corresponds to the earliest moment at which the cloud has reached its full development, thus ensuring a conservative estimate (further details are reported in the Supplementary Materials).

The results show that the total evaporated fraction ($M_{EVAP\%}$) is substantially higher when pool formation is considered (*wall-film* condition) compared to the cascade-only case (*escape* condition). This difference is reflected not only in the source term but also in the spatial extension of the vapour cloud and the associated damage distances. The effect is clearly visible in Fig. 6, which compares the iso-surfaces corresponding to ½ LFL for Case 1 (*escape*) and Case 2 (*wall-film*).

Since, as can be seen in Fig. 6, the presence of the pool leads to the formation of a much larger cloud than that resulted only by the evaporation of the cascade alone, it was chosen for all the subsequent simulations, not to neglect the contribution due to the evaporation of the liquid pool, using the "*wall-film*" model.

Discussion regarding the splash parameter is reported in Section 2. Having no experimental data available for comparison, it was chosen to neglect the splash phenomenon. The latter hypothesis leads to a significant reduction of computational costs in terms of both time and memory occupied.

Table 2
Results of simulation with boundary condition of "Escape", i.e., only cascade, and "Wall-Film", i.e., cascade and pool evaporation, at release end.

	Case 1 (Escape) Cascade only	Case 2 (Wall-Film) Cascade + pool	Variation Δ
$M_{EVAP\%}$ [%]	11.8	66.6	+54.8
$d^{BUND}_{x+LFL/2}$ [m]	10.8	34.9	+24.1
$d^{RELEASE}_{z\pm LFL/2}$ [m]	15.7	36.6	20.9

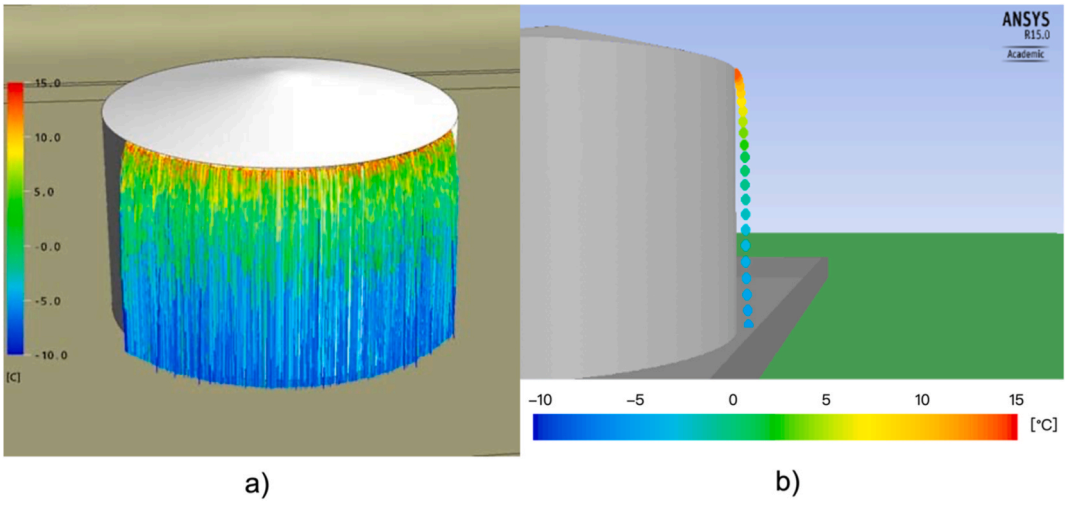

Fig. 4. Drop temperature [°C] predicted by (Atkinson and Gant, 2012a) (a) and in this work (b).

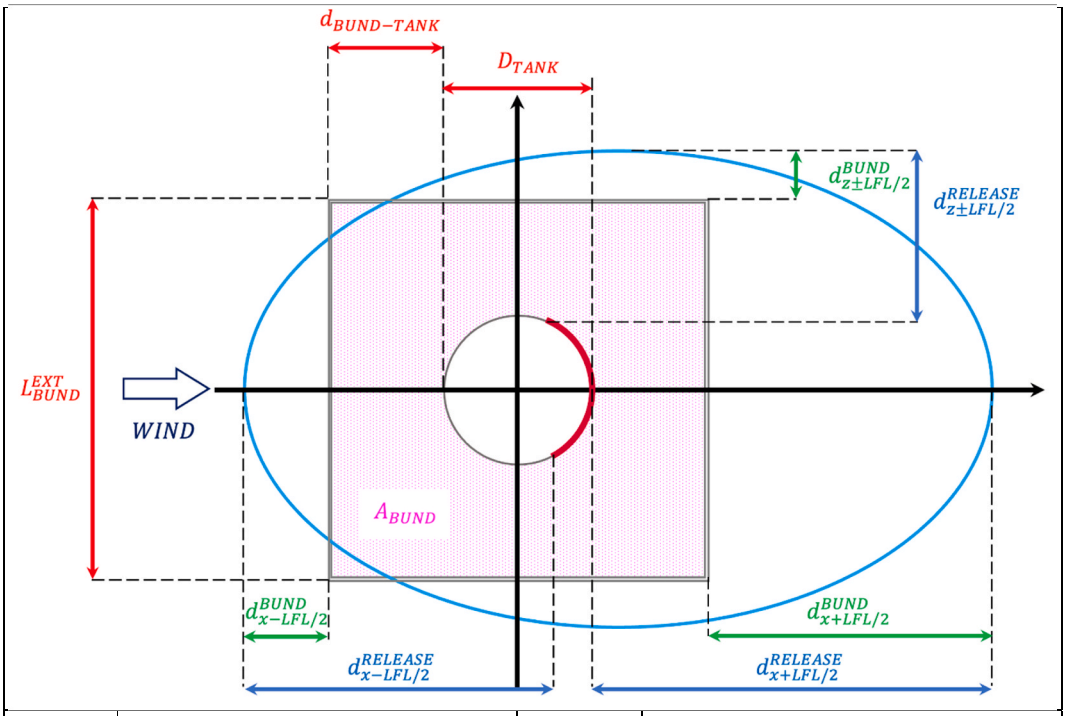

$d^{BUND}_{x+LFL/2}$	Maximum distance in the direction of release reached by the cloud bounded by an iso-surface with a concentration equal to LFL/2, measured from the outer bund walls	$d^{RELEASE}_{x+LFL/2}$	Maximum distance in the direction of release reached by the cloud bounded by an iso-surface with a concentration equal to LFL/2, measured from the centre of the release
$d^{BUND}_{x-LFL/2}$	Maximum distance in the opposite direction from release reached by the cloud bounded by an iso surface with a concentration of LFL/2, measured from the outer walls of the bund	$d^{RELEASE}_{x-LFL/2}$	Maximum distance in the opposite direction from release reached by the cloud bounded by an iso surface with a concentration of LFL/2, measured from the centre of the release
$d^{BUND}_{z+LFL/2}$	Maximum distance in wind transverse direction reached by the cloud bounded by an iso-surface with a concentration equal to LFL/2, measured from the outer bund walls	$d^{RELEASE}_{z\pm LFL/2}$	Maximum distance in wind transverse direction reached by the cloud bounded by an iso-surface with a concentration equal to LFL/2, measured the from the centre of the release
H_{TANK}	Tank height	$d_{BUND-TANK}$	Distance between the bund internal walls and the tank shell
D_{TANK}	Tank diameter	H_{BUND}	Bund walls height
A_{BUND}	Useful bunded surface area	H^{+}_{BUND}	Portion of the bund walls height that is above the ground (for buried basin)
L^{EXT}_{BUND}	Lateral length of the bund	H^{-}_{BUND}	Portion of the bund walls height that is under the ground (for buried basin)

Fig. 5. Characteristic distances useful for the purpose of estimating the damage area.

4.2. Sensitivity analysis to the thermal boundary condition of the "wall-film" model

The setting of thermal boundary conditions (BCs) at solid surfaces may influence model predictions in two ways. First, for the gaseous phase, wall temperature can affect near-wall buoyancy-driven and convective flows, potentially modifying the overall flow field, particularly under low wind speed conditions. Second, for the condensed phase, wall temperature governs heat exchange with impinging droplets and with the liquid film formed at the basin floor.

For simulations employing the "*escape*" boundary condition, where droplets do not interact with solid surfaces, the thermal BC at the ground has negligible influence. In contrast, under the "*wall-film*" condition, the liquid film in contact with the soil can exchange heat with the underlying surface, thereby affecting the evaporation rate and overall vapour generation.

To assess the sensitivity of the model to this parameter, two additional simulations were performed differing only in the thermal boundary condition applied to solid surfaces: adiabatic in one case and isothermal in the other. The corresponding results are summarized in Table 3. As expected, the total evaporated mass is slightly higher in the isothermal case, whereas the fraction of released mass accumulating within the basin ($M_{WF\%}$) is marginally higher under adiabatic conditions. However, the differences between the two configurations is very limited, indicating that the thermal BC exerts only a minor influence on the key output parameters.

On this basis, the isothermal boundary condition was adopted for all subsequent simulations to ensure modelling consistency and computational stability across the parametric study.

Following the sensitivity assessments, a reference CFD model was defined for the systematic investigation of bund geometric parameters; its main characteristics are reported in Table 4. An identical simulation procedure was applied to all analysed configurations, consisting of three sequential phases, summarized in Table 5.

The first phase involves the convergence of the wind profile. In this stage, only the airflow and turbulence quantities (turbulent kinetic

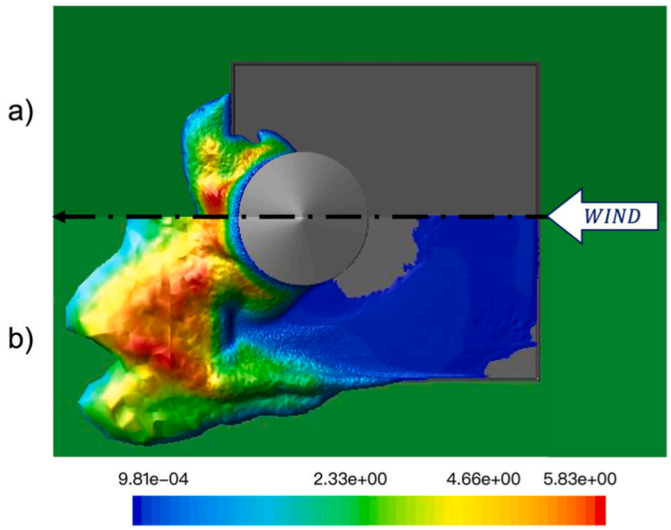

Fig. 6. Cloud bounded by an iso-surface with a concentration equal to LFL/2 for Case 1 (a) and Case 2 (b); the colours are representative of the depth [m] of the cloud. (For interpretation of the references to colour in this figure legend, the reader is referred to the Web version of this article.)

Table 3
Results of sensitivity analysis on soil thermal condition.

	Case 3	Case 4	Variation Δ%
Thermal condition on the soil	Adiabatic	Isotherm $T_{soil} = T_{air} =$ 273.16 [K]	-
$M_{EVAP\%}$ [%]	49.8	50.7	+0.9
$M_{WF\%}$ [%]	32.8	32.3	−0.5

Table 4
CFD model used for source term estimation.

DPM Boundary-Condition on the wall	Wall-Film
Splash parameter	0
Tank Thermal Boundary-Condition	Isothermal; $T^{\circ}_{DROPS} = 288.15$ [K]
Soil and bund thermal Boundary-Condition	Isothermal; $T_{AIR} = 273.15$ [K]
Weather conditions	5D

energy and its dissipation rate) are solved until convergence within the computational domain. The solver operates in stationary and the multiphase DPM model is deactivated.

The second phase represents the active release. Vapour generation results from two concurrent mechanisms: evaporation from the falling liquid cascade and evaporation from the liquid pool formed within the basin. The solver is switched to transient mode and the DPM model is activated.

The third phase corresponds to post-release dispersion. After termination of the liquid discharge, evaporation continues exclusively from the pool remaining within the containment basin. Following a short transient required for suspended droplets to settle, pool evaporation becomes the sole vapour source. The solver remains in transient mode, with the DPM model active but without further droplet injection.

Table 5
Summary of the 3 phases of simulations.

	1st phase	2nd phase	3rd phase
	Convergence of the atmospheric model	Release simulation	Post-release simulation
Solver	Stationary	Transient	Transient
Duration of the simulation	-	20 [s]	20[s]
DPM model	Disabled	Enabled	Enabled
Injection del DPM	-	Enabled	Disabled
Evaporative contribution	-	Cascade evaporation Pool evaporation	Pool evaporation

4.3. Analysis of the influence of a second upstream tank

The first configuration analysed in this work (1T) corresponds to the reference case reported in the "RR937" Report (Atkinson and Gant, 2012a), which reproduces the geometry of the storage tank and containment basin involved in the Buncefield accident. This configuration was used for model validation and for the grid independence analysis.

Since the objective of the present study is to assess the performance of containment systems, the broader layout of the Buncefield facility was not reproduced. Restricting the computational domain to the tank–bund system allows for a more focused investigation of vapour generation and dispersion mechanisms associated with the containment geometry, independently of site-specific complexities.

In the base configuration (1T), the tank is eccentrically positioned within the basin, with a minimum clearance of 3 m from the nearest bund walls. Although the original report does not explicitly justify this layout, such arrangements are consistent with bunds designed to accommodate multiple tanks, a configuration historically common in industrial plants.

To evaluate the influence of multiple tanks within the same containment basin, a second tank (2T configuration) was introduced upstream of the releasing tank. The second tank was assumed to have identical dimensions, with the same 3 m clearance from the inner bund walls. The results obtained at the end of the release for the two configurations described are shown in Table 6.

From a purely geometric standpoint, the presence of a second tank reduces the free area available for liquid pool spreading, which would be expected to decrease the evaporative surface and, consequently, the total evaporated fraction. However, the results indicate a slight increase in the evaporated mass when the second tank is present.

A similar trend is observed in the post-release phase, where the evaporation rate of the liquid film does not decrease despite the reduced pool area. This behaviour suggests that geometric obstruction effects are counterbalanced by modifications in the internal flow field. In particular, the wake generated by the upstream tank enhances local airflow velocities near the basin floor, thereby promoting increased convective mass transfer. This effect is illustrated in Fig. 7, which reports the horizontal wind speed profile near the bund base during the release phase for cases 1T (a1) and 2T (a2). In the 2T configuration, the wake of the upstream tank alters the internal circulation and locally increases velocity levels.

The presence of the second tank also affects cloud dispersion patterns. As shown in Figure Fig. 8, the vapour cloud in configuration 2T exhibits a greater transverse expansion compared to the single-tank case, reflecting the influence of wake-induced flow deflection on plume development at the time of maximum cloud extension.

Table 6
Results of sensitivity analysis on the presence of a secondary tank upstream.

	Case 1T (Single Tank)	Case 2T (Double Tank)
$M_{EVAP\%}(t = 20[s])$ [%]	66.6	68.9
$d^{BUND}_{x+LFL/2}$ [m]	56.9	50.7
$d^{BUND}_{z\pm LFL/2}$ [m]	19.9	21.7

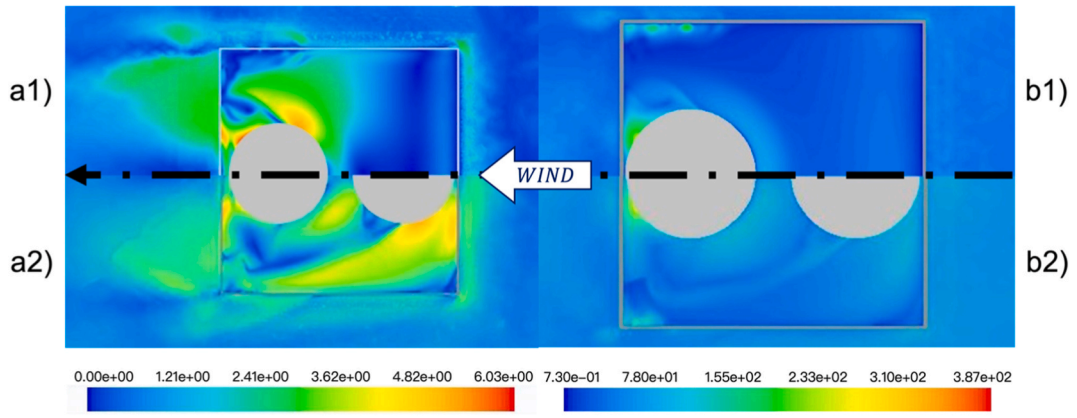

Fig. 7. Horizontal wind profile [m/s] @ 0.2 [m] near the bund for Case 1T (a1) 2T (a2) and horizontal profile of turbulence intensity [-] @ 0.2 [m] near the bund for Case 1T (b1) 2T (b2).

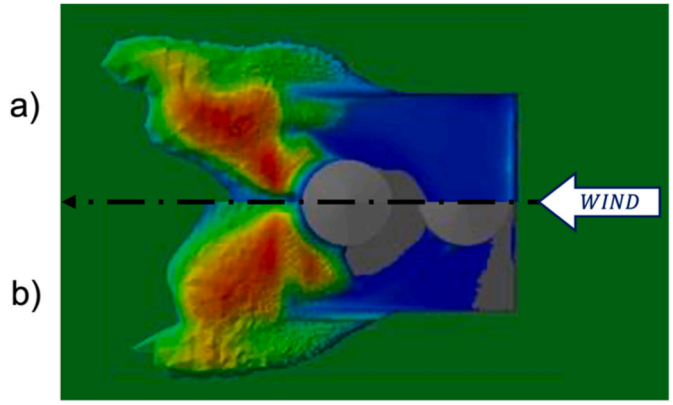

Fig. 8. Cloud delimitated by an iso-surface with concentration equal to LFL/2 for Case 1T (a) and Case 2T (b); the colours are representative of the depth [m] of the cloud. (For interpretation of the references to colour in this figure legend, the reader is referred to the Web version of this article.)

4.4. Analysis of the influence of the bund geometric parameters

In the subsequent configurations, the overall geometry of the system was maintained, except for the placement of a single tank at the centre of the basin. This layout is more representative of current design practice and aligns with contemporary regulatory guidance, which generally discourages the installation of multiple tanks within the same containment basin depending on tank capacity and stored substance (HSG176, 2015).

The analysis focused on two geometric parameters with direct safety relevance: (i) bund wall height and (ii) effective bund surface area.

Bund wall height plays a fundamental role in vapour containment, as the walls act as physical barriers against which the dense flammable cloud impinges. If sufficiently high, they can significantly delay or partially prevent vapour overflow, thereby reducing the likelihood of off-site consequences. From a fire safety perspective, this is particularly relevant because, provided that regulatory requirements are met, ignition sources should not be present within the basin boundaries.

The effective bunded surface determines the maximum pool area achievable during the release. Since the evaporation rate of a liquid pool strongly depends on its exposed surface area, a reduction in basin surface may theoretically lead to lower evaporation rates and reduced vapour generation.

To investigate the influence of these two parameters (i.e., the bund walls height and the bunded surface), three different containment configurations were implemented, their main features are reported in Table 7. In addition to the base case (1.8 m wall height), a 3.6 m wall configuration was analysed to explore the influence of increased vertical confinement within the limits permitted by applicable regulations ((CM 22/12/62, nd)National Fire Protection Association, 2024). The resulting source terms and maximum damage distances at the end of release are reported in Table 8.

Increasing bund wall height produces a marked reduction in damage distances, particularly in the downwind direction. This effect is not solely attributable to the geometric barrier provided by the walls but also to modifications in the internal flow field. A wall height of 1.8 m, consistent with NFPA recommendations, is insufficient to prevent vapour overflow: once the cloud reaches the wall crest, it spills out relatively easily. Conversely, a height of 3.6 m, which is still within the maximum height limits prescribed by current legislation, enhances vapour confinement, although complete containment is not achieved, as shown in Fig. 9, where a comparison between case BUND 1 (i.e., the base case) and BUND 2 and between BUND 1 and BUND 3 is reported.

In Fig. 10 the turbulence intensity profile on the vertical plane of symmetry of the domain is shown: it can be noted that higher walls alter the flow structure both within and downstream of the basin. In particular, the elevated configuration promotes stronger turbulence in the wake region beyond the bund. The dense vapour cloud, flowing over the crest under gravity-driven motion, gains additional momentum due to the greater elevation difference, enhancing mixing with ambient air. This increased dilution contributes, together with changes in the cloud movement, to the observed reduction in damage distances.

The influence of bund surface area was evaluated by comparing configurations BUND 2 and BUND 3, which share the same wall height but differ in basin footprint. Reducing the bunded surface does not produce a significant variation in the total evaporated mass at the end of release, as $M_{EVAP\%}$ remains nearly unchanged between the two cases. Although a larger pool area would theoretically favour higher evaporation rates, this effect appears secondary compared to the influence of wall height on the internal flow field.

Indeed, increased wall height modifies turbulence levels within the basin, affecting vapour accumulation and concentration gradients above

Table 7
Main geometric characteristics of the three containment configurations.

Case	BUND 1	BUND 2	BUND 3
$d_{BUND\text{-}TANK}$ [m]	19.2	19.2	11.25
L^{EXT}_{BUND} [m]	64.6	64.6	48.7
H_{BUND} [m]	1.8	3.6	3.6
A_{BUND} [m^2]	3528.8	3528.8	1764.4
V_{BUND}	110%V_{TANK}[a]	220%V_{TANK}	110%V_{TANK}[a]

[a] volume equal to 110% of the tank capacity as required by the standard HSG176.

Table 8
The results obtained, both in terms of assessment of the source term at the end of the release and the maximum extension of the damage area.

Case	BUND 1	BUND 2	BUND 3
$M_{EVAP\%}$ [%]	64.3	34.3	34.9
$d^{RELEASE}_{x+LFL/2}$ [m]	79	43.1	44.5
$d^{BUND}_{x+LFL/2}$ [m]	59.2	23.3	32.6

the liquid pool. Since evaporation is driven by the concentration difference between the liquid surface and the surrounding atmosphere, flow-field effects associated with wall height dominate over purely geometric surface-area effects. As a result, the transition from BUND 1 (1.8 m) to BUND 2 and BUND 3 (3.6 m) produces a substantial change in evaporated mass and damage distances, whereas the difference between BUND 2 and BUND 3 is comparatively minor. This indicates that bund wall height is the predominant design parameter influencing hazard extent.

The downwind distance corresponding to ½ LFL is similar for BUND 2 and BUND 3 when measured from the release point. A comparable trend is observed in the transverse direction, with even smaller deviations between configurations. Assuming the absence of ignition sources within the basin, these external distances represent the effective damage range; under this assumption, the configuration with larger basin surface may offer a slight advantage in limiting external hazard propagation.

However, it should be noted that an increased basin surface also implies a larger potential pool-fire area in the event of ignition. Since pool-fire radiation distances scale with burning surface, larger basins may generate more severe thermal radiation effects. Therefore, when adopting extended containment surfaces, additional mitigation measures, such as fixed or semi-fixed foam injection systems, should be considered to reduce the probability and consequences of pool fires.

4.5. Tank placement below the ground level

A review of existing containment layouts indicates that, in some installations, bunds are partially or fully located below ground level. Current regulations allow this configuration but do not provide explicit design prescriptions. For instance, the maximum bund wall height prescribed by Italian legislation (4 m) is explicitly referenced to ground level; therefore, increasing effective containment height through partial burial may formally comply with regulatory limits.

However, underground configurations introduce additional technical considerations. Excessive burial depth, particularly in relation to groundwater level, may lead to rainwater accumulation within the basin, requiring pumping systems for drainage. Pump failure, which cannot be considered a rare event, may result in significant water accumulation, potentially generating secondary risk scenarios that should be included in a comprehensive safety assessment. On the other hand, partial burial may offer operational advantages, such as improved visual inspection of the tank and easier emergency intervention due to reduced wall elevation above ground.

To evaluate the influence of basin burial on vapour dispersion and damage extent, two additional configurations, BUND B1 and BUND B2, were analysed and compared with the corresponding above-ground cases BUND 1 and BUND 3. Their main characteristics are shown in Table 9 and schematically represented in Fig. 11. In both BUND B1 and BUND B2, the basin volume was maintained equal to 110% of tank capacity, as required by standards. In configuration BUND B1, the bund

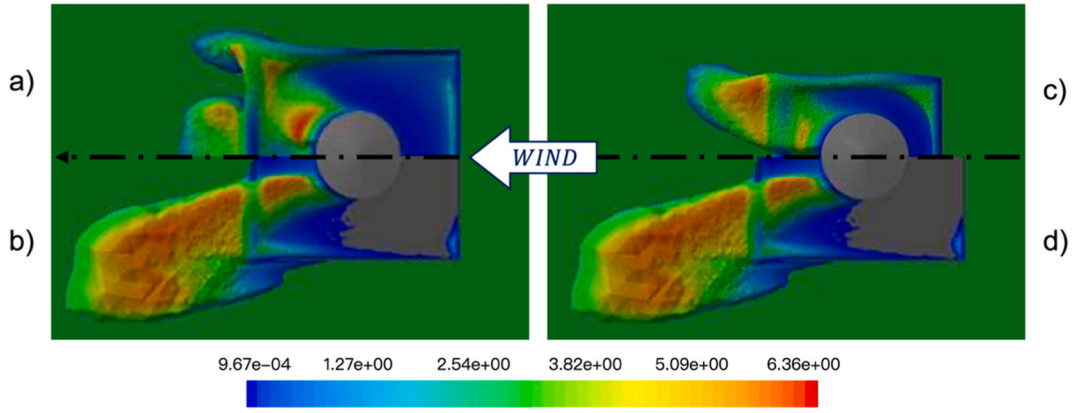

Fig. 9. Cloud delimitated by an iso-surface with concentration equal to LFL/2 at its maximum extension for BUND 2 (a) and BUND 1 (b), and BUND 3 (c) and BUND 1 (d); the colours are representative of the depth [m] of the cloud. (For interpretation of the references to colour in this figure legend, the reader is referred to the Web version of this article.)

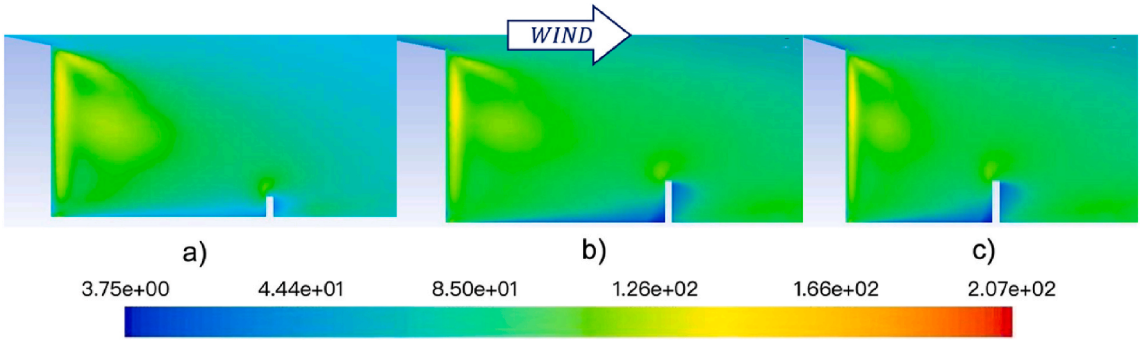

Fig. 10. Vertical profile on symmetry plane (z = 0) of turbulence intensity for case BUND 1 (a), BUND 2 (b) and BUND 3 (c).

Table 9
Main geometric characteristics of the two containment configurations placed below ground level.

Case	BUND B1	BUND B2
V_{BUND}, [m^3]	110% V_{TANK}	110% V_{TANK}
H_{BUND}, [m]	1.8	3.6
H^{y+}_{BUND}, [m]	0	1.8
H^{y-}_{BUND}, [m]	1.8	1.8
A_{BUND}, [m^2]	3528.8	1764.4

wall height is 1.8 m and the basin is entirely below ground level. In configuration BUND B2, the total wall height is 3.6 m, but only half of it is buried, resulting in a lower effective basin surface to preserve the required containment volume. Further burial was not considered in this case to avoid triggering additional regulatory requirements related to work at height (D.Lgs. 81/08).

The results, reported in Table 10, show that basin burial has negligible influence on the total vapour source term. In contrast, it significantly affects damage distances. Compared to the corresponding above-ground configurations with equal bund surface, both BUND B1 and BUND B2 exhibit increased downwind distances measured from the release point. This behaviour can be attributed to the reduced aerodynamic influence of bund walls when they are located wholly or partially below ground level. Above-ground walls promote turbulence generation and enhance mixing when the dense cloud flows over the crest. When the basin is fully buried (BUND B1), this mechanism is essentially absent, and the internal flow resembles that of an open terrain configuration. Consequently, BUND B1 appears less effective not only relative to BUND 1 but also compared to BUND B2.

In configuration BUND B2, where half of the wall height remains above ground, partial aerodynamic interaction is preserved. The cloud flowing over the crest undergoes vertical displacement and subsequent gravitational descent, which enhances mixing and dilution. Nevertheless, BUND B2 remains less effective than the fully above-ground high-wall configuration (BUND 3).

Flow-field analysis (Fig. 12) indicates that both underground configurations show a greater tendency for the cloud to dilute in the area in front of the bunding; this is probably due to the greater turbulence near the ground in the area downstream of the bunding induced by the bunding wake. The reduced wall protrusion decreases turbulence generation at the crest but promotes broader dispersion downstream, altering cloud morphology (Fig. 13). In addition to increased downwind distances, underground basins also show a larger overall damage area, primarily due to lower internal wind speeds in the upstream region of the basin, which limit dilution during the early dispersion phase.

Overall, the results indicate that although basin burial does not significantly affect vapour generation, it weakens the aerodynamic containment effect of bund walls and may therefore increase external hazard distances.

Table 10
Results, both in terms of source term and extension of the damage area, obtained for the two containment configurations placed below ground level.

Case	BUND 1	BUND B1	BUND 3	BUND B2
$M_{EVAP\%}$, [%]	64.3	64.3	34.9	34.8
$d^{RELEASE}_{x+LFL/2}$, [m]	79	86	44.5	52.6
$d^{BUND}_{x+LFL/2}$, [m]	59.2	66.2	32.6	40.7

4.6. Introduction of anti-overtopping deflectors

A comprehensive safety assessment of storage tanks must account for all relevant structural failure modes. Two representative scenarios are catastrophic tank rupture and cracking in the lower part of the shell, the latter often associated with the overtopping phenomenon. Based on experimental investigations (Atherton, 2005), the overtopping liquid fraction can be estimated through the following empirical correlation:

$$Q_{overtopping} = A \exp\left[-B\left(\left(H_{BUND}/H_{TANK}\right)\right)\right]$$

where the constants A and B depend on the tank capacity (whose dimensions have been set to standard values in the present study), the angle of inclination of the anti-overtopping deflectors with respect to the horizontal plane θ_{BUND_WALL} (see Fig. S3 of the Supplementary Material), the ratio between the tank radius (R_{TANK}) and the tank heigh (H_{TANK}) and the failure mode considered. The correlation, which is applicable to both circular and rectangular bunds, provides reliable results in the range:

$$0.66 \leq \left(\frac{R_{BUND} - R_{TANK}}{R_{TANK}}\right) \leq 5.32$$

Where R_{BUND} is the bund radius.

The above expressions indicate that, for a given storage capacity, overtopping mitigation primarily depends on bund wall height. For catastrophic rupture, assumed here as the most conservative failure mode, increasing wall height from 1.5 m to 3.5 m reduces the overtopping fraction from 72.8% to 32.6% (Nair, 2008), although the residual fraction remains significant. Further height increases yield diminishing improvements.

Table 11 reports the overtopping fractions estimated for selected configurations analysed in this study. A tank-to-bund radius ratio close

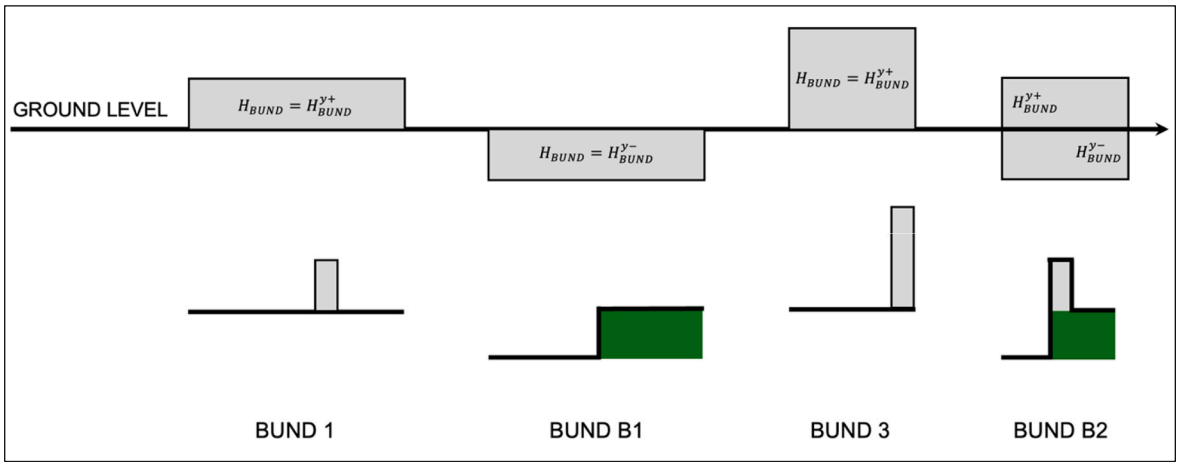

Fig. 11. Configurations analysed for the study of the influence of the burial of the basin.

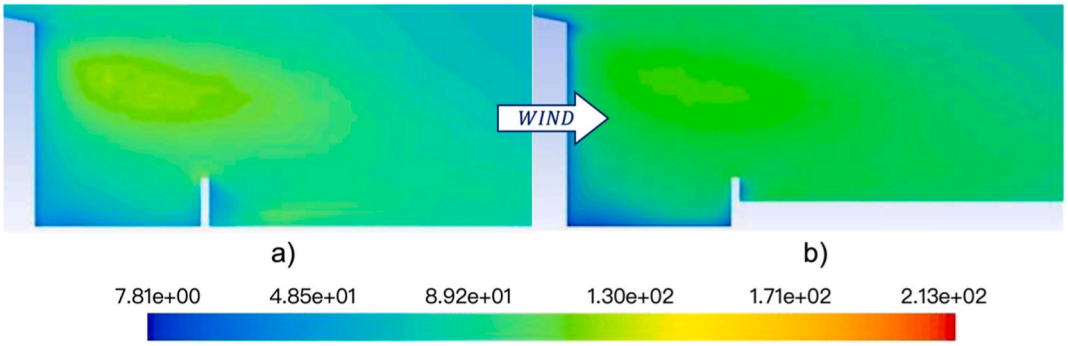

Fig. 12. Vertical profile on the symmetry plane (z = 0) of turbulence intensity for case BUND 3 (a), BUND B2 (b).

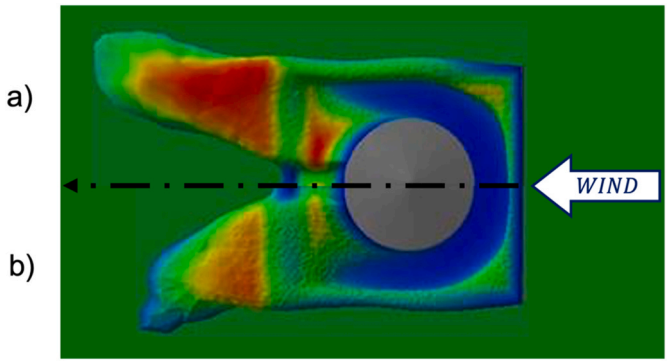

Fig. 13. Cloud delimitated by an iso-surface with concentration equal to LFL/2 for case BUND B2 (a) and BUND 3 (b) at its maximum extension; the colours are representative of the depth [m] of the cloud. (For interpretation of the references to colour in this figure legend, the reader is referred to the Web version of this article.)

to unity was assumed, and catastrophic rupture was considered as the reference failure mode to obtain conservative results.

To further reduce overtopping, previous studies have proposed the installation of deflectors inclined at 45° toward the inside of the basin (Nair, 2008), which can reduce the overflowing fraction to negligible values. However, deflectors may also modify the internal flow field and thus influence vapour generation and dispersion.

For this reason, 45° inward-inclined deflectors were added to a containment basin geometrically equivalent to configuration BUND 1. The results are reported in Table 12and compared with configurations BUND 1 and BUND 2.

The introduction of anti-overtopping deflectors (configuration BUND D-1) leads to a significant reduction in both source term and damage distances compared to the reference case (configuration BUND 1). However, it should be noted that this improvement cannot be attributed exclusively to the presence of the deflectors. In configuration BUND D-1, the combined wall-plus-deflector height is approximately 77% higher than that of BUND 1. Therefore, the observed mitigation effect results

Table 11
Estimated overtopping liquid fractions for the different bunding configurations considered.

	BUND 1	BUND 2	BUND 3
$\frac{R_{BUND} - R_{TANK}}{R_{TANK}}$	1.68	1.68	0.89
A	0.7918	0.4814	0.7918
B	2.6596	2.1866	2.6596
R_{BUND}, [m]	33.5	33.5	23.7
V_{BUND}, [m^3]	≈110% V_{TANK}	≈220% V_{TANK}	≈110% V_{TANK}
$Q_{overtopping\%}$, [%]	57.5	28.5	41.8

Table 12
Results at release end, both in terms of source term and extension of the damage area, obtained as a result of adding the deflectors. The results obtained previously with configuration BUND 1 are also shown for comparison purposes.

Case	BUND 1	BUND D-1	BUND 2
Wall height [m]	1.8	3.2	3.6
$M_{EVAP\%}$, [%]	64.3	41.2	34.3
$d^{RELEASE}_{x+LFL/2}$, [m]	79	62.7	43.1
$d^{BUND}_{x+LFL/2}$, [m]	59.2	42.9	23.3

from a coupled geometric modification, involving both the change in flow redirection induced by the deflectors and the increase in effective containment height.

The simulations show that the presence of deflectors alters the internal recirculation structure and increases turbulence intensity within the basin. While the deflectors clearly contribute to modifying the local flow structure, the present comparison does not allow a complete decoupling of their aerodynamic effect from the influence of increased effective height.

Nevertheless, the configuration with deflectors results in an increase in both the vapour source term and the associated damage distances when compared to BUND 2. In this comparison, the effective height of the wall–deflector system is approximately 0.4 m (≈11%) lower than that of BUND 2. While part of the variation in damage distances may be attributed to this reduced effective height, the increase in evaporation rate suggests that geometric inclination itself plays a significant role and that the effect cannot be entirely ascribed to height differences.

This effect is particularly evident upstream of the tank (Fig. 14(b); see also Fig. S2 in the Supplementary Material) and downstream of the release, where the inclined surfaces induce additional air motion (Fig. 15). Compared to vertical walls, the deflectors promote stronger internal mixing both in the absence and in the presence of release.

The reduction in the damage distance in the case of vertical bund walls, compared to inclined ones, can be linked to two further phenomena. First, in the case of vertical walls, the dense cloud spilling over the crest undergoes a gravity-driven fall (as described in paragraph 4.4), enhancing turbulence and mixing downstream. This mechanism is less pronounced when the wall is inclined, since the deflector acts as a ramp that facilitates smoother cloud outflow, as already been found in the literature (Coldrick et al., 2011) for a bund with both side sloping walls. Second, the interaction between the tank wake and a vertical wall generates stronger downstream turbulence compared to the inclined configuration.

As a result, although deflectors are highly effective in reducing overtopping under catastrophic rupture conditions, they may simultaneously promote wider vapour dispersion by modifying the aerodynamic characteristics of the containment system. This highlights the need to evaluate hydraulic containment performance and vapour dispersion behaviour jointly when assessing bund design options.

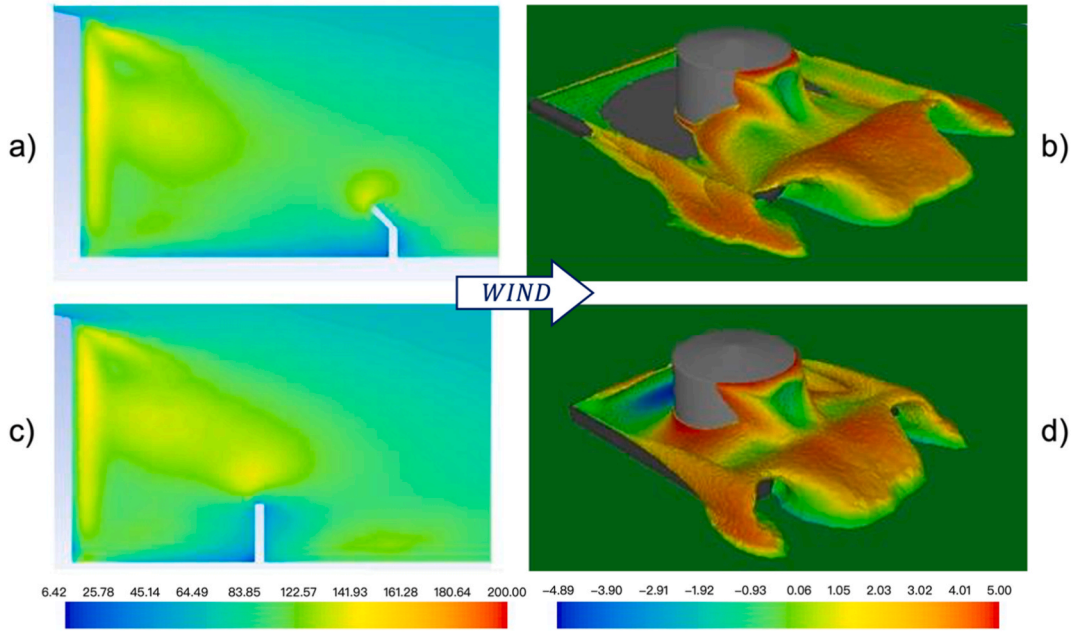

Fig. 14. Vertical profile on the symmetry plane (z = 0) of turbulence intensity for case BUND D-1 (a) and BUND 3 (c) and cloud delimitated by an iso-surface with concentration equal to LFL/2 for case BUND D-1 (b) and BUND 3 (d); the colours are representative of the depth [m] of the cloud. (For interpretation of the references to colour in this figure legend, the reader is referred to the Web version of this article.)

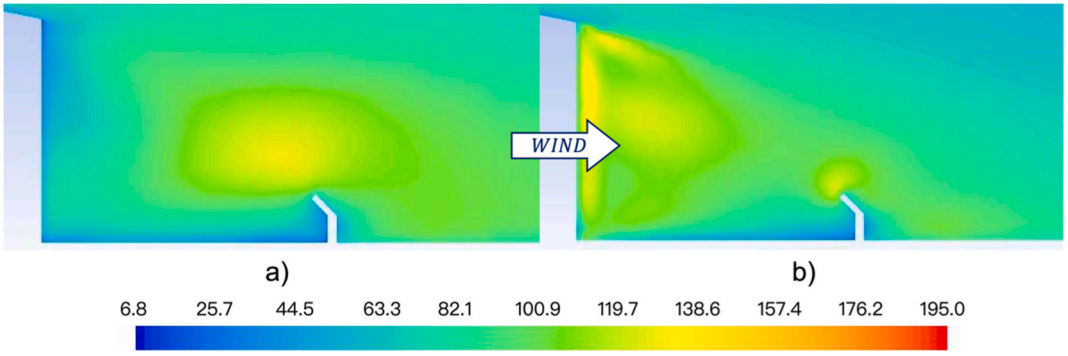

Fig. 15. Vertical profile on the symmetry plane of turbulence intensity for BUND D-1 in absence (a) and presence (b) of the cloud.

4.7. Analysis of the influence of wind direction

In this section, the influence of wind direction relative to the release location was analysed to identify the worst-case configuration in terms of maximum damage area. Using the same containment geometry as configuration BUND 3, two additional scenarios were simulated, differing only in wind orientation with respect to the release location: (i) BUND 3-LW, considering transverse wind, with the incoming flow forming a 90° angle relative to the normal direction of the release; (ii) BUND 3-UW, considering upwind configuration, where the wind directly impinges on the release location.

The results are summarized in Table 13 and compared with the base case BUND 3 (downwind configuration).

The total vapour production ($M_{EVAP\%}$) is highest in the upwind configuration (BUND 3-UW), followed by the transverse case (BUND 3-LW), and lowest in the base case where the release is located downwind. This behaviour can be attributed to enhanced air entrainment in the region close to the release when the wind directly interacts with the discharge zone. In the upwind configuration, the incoming flow increases local turbulence levels (Fig. 16), promoting convective mass transfer and consequently increasing evaporation rates.

Fig. 17 compares the spatial extent of the damage area for configurations BUND 3 and BUND 3-UW (left) and for BUND 3-LW (right). The results clearly indicate that wind orientation relative to the release plays a significant role in determining both source term intensity and cloud propagation patterns.

Table 13
Results of the analysis of the influence of wind direction.

Case	BUND 3 (Downwind)	BUND 3-LW (Lateral-Wind)	BUND 3-UW (Upwind)
$M_{EVAP\%}$, [%]	34.9	40.9	47.6
$d^{RELEASE}_{x+LFL/2}$, [m]	44.5	72.7	96.3
$d^{BUND}_{x+LFL/2}$, [m]	32.6	48.3	59.4

The maximum damage distances are also observed for the upwind configuration. When the wind blows toward the tank, the cloud is partially obstructed by the tank structure, which modifies its initial development. The vapour accumulates temporarily along the symmetry plane and spreads laterally before being entrained downstream by the tank wake (Fig. 17 b). This combined obstruction–wake interaction

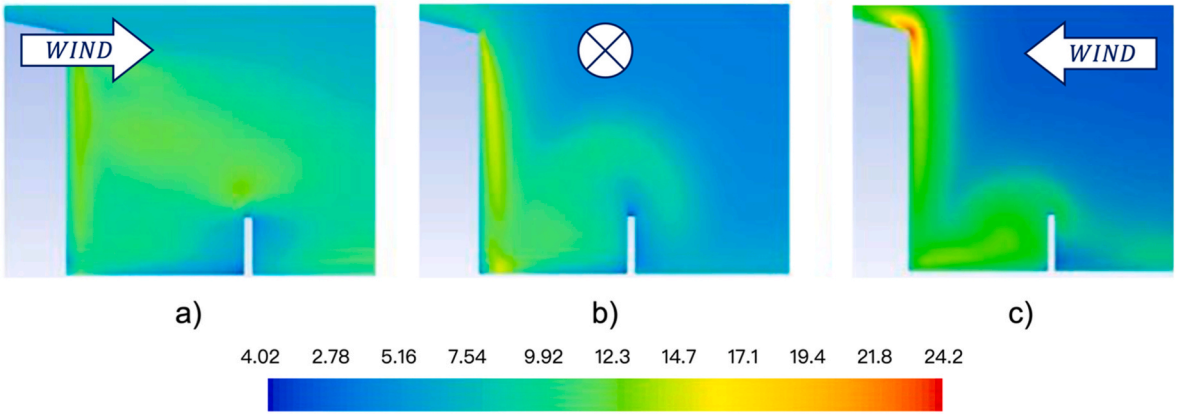

Fig. 16. Vertical profiles of the turbulence intensity on a plane passing through the centre of release for case BUND 3 (a) and BUND 3-UW (c), where the arrow indicates the direction of wind coming from, and for case BUND 3-LW (b) where the wind is perpendicular to the section plane.

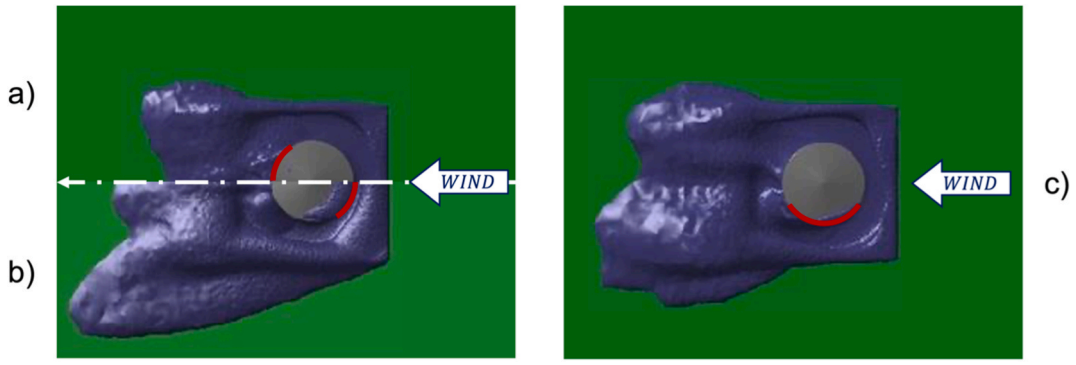

Fig. 17. Surface with a concentration higher than LFL/2 for case BUND 3 (a), BUND 3-UW (b), and BUND 3-LW (c). The red marks indicate the releases. (For interpretation of the references to colour in this figure legend, the reader is referred to the Web version of this article.)

enhances cloud extension both laterally and downwind.

In the transverse configuration (BUND 3-LW), the damage distances are larger than in the base case but smaller than in the upwind scenario. Although vapour production is lower than in BUND 3-UW, the lateral wind promotes asymmetric cloud spreading, increasing the overall affected area compared to the downwind case.

5. Conclusions

This study investigated the influence of different bund configurations on gasoline vapour cloud generation and dispersion following a tank overfilling scenario through CFD simulations. The analysis focused on how geometric modifications of the containment system alter the internal flow field, air entrainment in the cloud, dilution and consequently the extent of the damage area.

The efficiency of each configuration was evaluated considering both the vapour source term and the damage distance, defined as the distance – measured from the bund walls, under the assumption that no ignition sources are present inside the basin – at which concentrations exceed regulatory thresholds such as ½ LFL.

A key outcome of the study is the demonstrated importance of including pool evaporation in the modelling of overfilling scenarios. The present results show that neglecting pool evaporation leads to a substantial underestimation of vapour production. The total evaporated mass increases from 11.8% in the cascade-only configuration to 66.6% when the liquid pool is included. Furthermore, the two evaporation processes, that of the cascade and that of the pool, cannot be decoupled in a comprehensive consequence assessment.

The sensitivity analysis on wall thermal boundary conditions (isothermal vs. adiabatic) revealed only a minor influence on evaporation rates, suggesting that mass transfer driven by concentration gradients plays a more significant role than heat transfer effects under the investigated conditions.

Regarding geometric parameters, the different basin configurations are summed up in Fig. 18, and the results obtained in term of damage distance are given in Table 14.

Bund wall height was identified as the dominant factor affecting damage distance, as higher walls enhance vapour confinement and modify the internal flow field, promoting dilution and reducing external hazard distances. Increasing bund wall height from 1.8 m to 3.6 m reduces downwind ½ LFL distances by approximately 45%. However, even raising the bund walls to heights close to regulatory limits is not sufficient to fully contain the cloud; additional mitigation systems, such as active barriers placed downstream of the basin, could enhance dilution of the cloud emerging from the bund walls. In contrast, variations in bund surface area have a comparatively secondary effect, since flow-field modifications induced by wall height prevail over purely geometric surface-area considerations.

Underground basin configurations were found to reduce the aerodynamic effectiveness of bund walls, decreasing turbulence and mixing and resulting in increased damage distances of up to 9%, despite negligible changes in the vapour source term.

The introduction of anti-overtopping deflectors on 1.8 m-high bund walls led to a clear reduction in both the source term and the damage distances (by approximately 20%). However, the resulting damage distances remain larger compared to those obtained with vertical-wall configurations of 3.6 m height. The inclination of the deflectors induces greater air recirculation within the basin, leading to increased

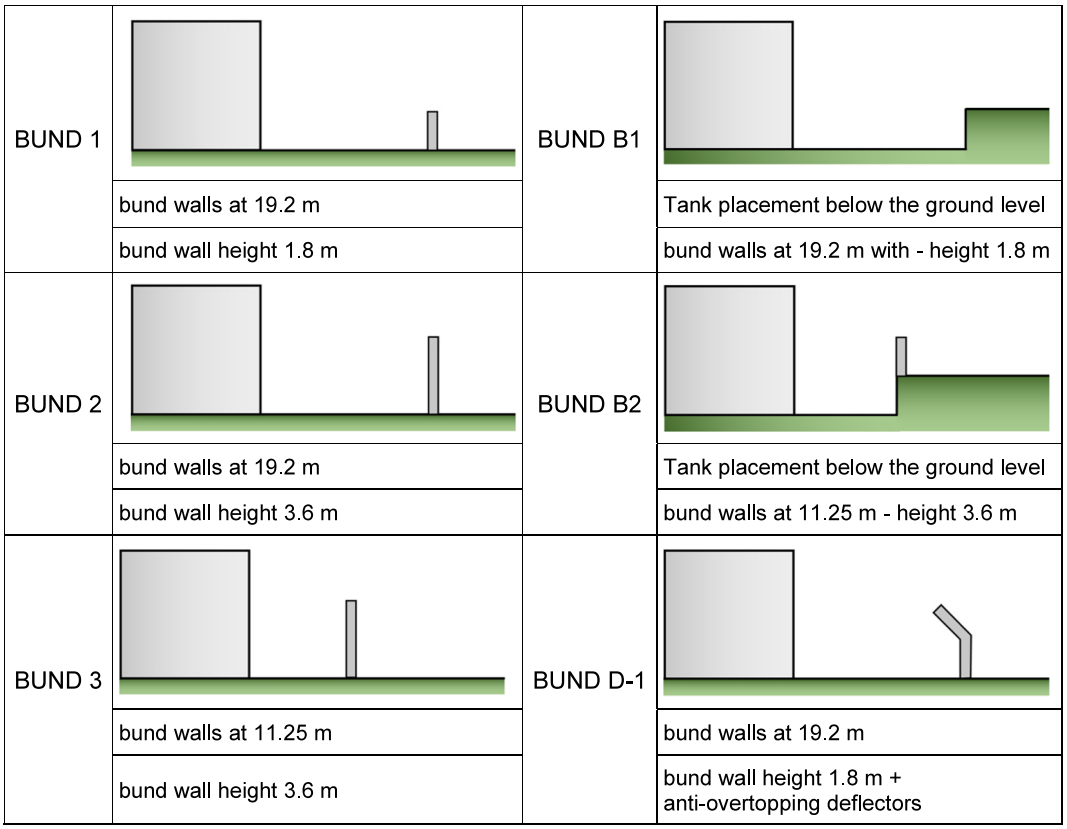

Fig. 18. Sum up of the different containment configurations.

Table 14
Variation of damage distances for each studied configuration compared to the base case BUND 1.

CASE		BUND 1	BUND 2	BUND 3	BUND 2T	BUND B1	BUND B2	BUND D-1	BUND 3 - LW	BUND 3 - DW
Start of lethality (LFL/2) [m]	$d_{x+LFL/2}^{RELEASE}$	79.0	43.1	44.5	54.3	86.0	52.6	62.7	72.7	96.3
	$d_{x+LFL/2}^{BUND}$	59.2	23.3	32.6	50.7	66.2	40.7	42.9	48.3	59.4
Variation Δ in respect to BUND 1 [m]	$d_{x+LFL/2}^{RELEASE}$	-	−35.9	−34.6	−24.7	7.0	−26.5	−16.3	−6.3	17.3
	$d_{x+LFL/2}^{BUND}$	-	−35.9	−26.6	−8.5	7.0	−18.5	−16.3	−10.9	0.2
Percentage deviation δ% in respect to BUND 1 [%]	$d_{x+LFL/2}^{RELEASE}$	-	−45.4%	−43.7%	−31.3%	8.9%	−33.5%	−20.6%	−8.0%	21.8%
	$d_{x+LFL/2}^{BUND}$	-	−60.6%	−44.9%	−14.4%	11.8%	−31.3%	−27.5%	−18.4%	0.3%

evaporation and improved mixing compared to the base-case BUND 1, although not as effectively as the 3.6 m vertical-wall configuration. The turbulence increase introduced by the deflectors is partly offset by the presence of the dense cloud. Moreover, the inclined geometry tends to accelerate the cloud in the downwind direction, whereas dilution appears more pronounced in the case of vertical walls due to the vertical fall of the dense cloud.

Regarding wind direction, the worst-case scenario occurs when the wind directly impinges on the release location; while, the distances obtained under lateral wind conditions are comparable to those of the upwind configuration when measured from the release point, but smaller when measured from the bund walls.

In conclusion, the adopted CFD-based methodology provides a detailed representation of the coupled phenomena governing overfilling scenarios, including droplet evaporation, pool formation through the *wall-film* model, and turbulence–geometry interaction induced by bund configurations. This integrated approach allows the simultaneous evaluation of source term evolution and vapour cloud dispersion, overcoming the limitations of simplified models that typically treat evaporation and dispersion separately.

Nevertheless, certain limitations must be acknowledged. The hydrocarbon mixture was approximated as pure n-hexane, which, although commonly adopted in the literature, may not fully capture the thermophysical variability of real gasoline. Secondary droplet interactions were neglected, which may influence local evaporation dynamics. Moreover, only one atmospheric stability class and wind velocity were considered. Extending the analysis to different atmospheric stability classes and wind conditions would considerably broaden the scope of the work.

CRediT authorship contribution statement

Fabrizio Santamato: Writing – original draft, Visualization, Validation, Investigation. **Carmelo Sofia:** Writing – original draft, Methodology, Investigation, Formal analysis. **Valentina Busini:** Writing – review & editing, Supervision, Resources, Data curation, Conceptualization.

Declaration of competing interest

The authors declare that they have no known competing financial interests or personal relationships that could have appeared to influence the work reported in this paper.

Appendix A. Supplementary data

Supplementary data to this article can be found online at https://doi.org/10.1016/j.jlp.2026.105999.

Data availability

Data will be made available on request.

References

ANSYS, 2013. ANSYS Fluent Tutorial Guide - Release 15.0.

API 650, 2012. American Petroleum Institute: Welded Tanks for Oil Storage.

API 2350, 2005. American Petroleum Institute: Overfill Protection for Storage Tank in Petroleum Facilities.

Atherton, W., 2005. An Experimental Investigation of Bund Wall Overtopping and Dynamic Pressures on the Bund Wall Following Catastrophic Failure of a Storage Vessel - Research Report, 333.

Atkinson, G., Coldrick, S., 2012. Vapour Cloud Formation: Experiments and Modelling - HSE Research Report 908.

Atkinson, G., Coldrick, S., Gant, S., Cusco, L., 2015. Flammable vapor cloud generation from overfilling tanks: learning the lessons from Buncefield. J. Loss Prev. Process. Ind. 35, 329–338. https://doi.org/10.1016/j.jlp.2014.11.011.

Atkinson, G., Gant, S., 2012a. Flammable Vapour Cloud Risks from Tank Overfilling Incidents - HSE Research Report 937.

Atkinson, G., Gant, S., 2012b. Buncefield Investigation: Liquid Flow and Vapour Production - HSE Research Report, 936.

Atkinson, G., Gant, S., Painter, D., Shirvill, L., Ungut, A., 2008. Liquid Dispersal and Vapour Production During Overfilling Incidents, 54. Institution of Chemical Engineers SympoSium SerieS.

BS 2654, 1984. British Standard: "Specification for Manufacture of Vertical Steel Welded Storage Tanks with butt-welded Shells for the Petroleum Industry.".

Busini, V., Lino, M., Rota, R., 2012. Influence of large obstacles and mitigation barriers on heavy gas cloud dispersion: A liquefied natural gas case-study. Industrial and Engineering Chemistry Research 51 (22), 7643–7650.

Busini, V., Rota, R., 2014. Influence of the shape of mitigation barriers on heavy gas dispersion. J. Loss Prev. Process. Ind. 29, 13–21. https://doi.org/10.1016/j.jlp.2014.01.001.

Chang, J.I., Lin, C.-C., 2006. A study of storage tank accidents. J. Loss Prev. Process. Ind. 19, 51–59. https://doi.org/10.1016/j.jlp.2005.05.015.

Cheng, Y., Jianyao, Y., Chen, S., Su, M., Zhang, Q., Liuchen, Y., Zhang, X., 2026. Physics-guided machine learning for evaporation risk assessment during gasoline spill accidents. J. Hazard. Mater. 502, 140610. https://doi.org/10.1016/j.jhazmat.2025.140610.

CM 22/12/62, n.d. Circolare Ministeriale 12/12/1962: Criteri Di Analisi E Valutazione Dei Rapporti Di Sicurezza Relativi Ai Depositi Di Gas E Petrolio Liquefatto (GPL), Official Journal of Italian Republic (Gazzetta Ufficiale), Rome (I).

Coldrick, S., Atkinson, G., Gant, S., 2010. Large Scale Evaporating Liquid Cascades - an Experimental and Computational Study.

Coldrick, S., Gant, S.E., Atkinson, G.T., Dakin, R., 2011. Factors affecting vapour production in large scale evaporating liquid cascades. Process Saf. Environ. Prot. 89, 371–381. https://doi.org/10.1016/j.psep.2011.07.004.

Derudi, M., Bovolenta, D., Busini, V., Rota, R., 2014. Heavy gas dispersion in presence of large obstacles: selection of modeling tools. Ind. Eng. Chem. Res. 53, 9303–9310. https://doi.org/10.1021/ie4034895.

Directive 2012/18/EU, n.d. Directive 2012/18/EU of the European Parliament and of the Council of 4 July 2012 on the Control of major-accident Hazards Involving Dangerous Substances, Amending and Subsequently Repealing Council Directive 96/82/EC Text with EEA Relevance.

D.Lgs. 81/08, n.d. "Testo Unico Sulla Salute E Sicurezza Sul Lavoro" - Attuazione Dell'Articolo 1 Della Legge 3 Agosto 2007, N. 123 in Materia Di Tutela Della Salute E Della Sicurezza Nei Luoghi Di Lavoro.

DM 15/5/96, n.d. Decreto Ministeriale 15/5/1996: Criteri Di Analisi E Valutazione Dei Rapporti Di Sicurezza Relativi Ai Depositi Di Gas E Petrolio Liquefatto (GPL). Official Journal of Italian Republic (Gazzetta Ufficiale), Rome (I).

DM 20/10/98, n.d. Decreto Ministeriale 20/10/1998: Criteri Di Analisi E Valutazione Dei Rapporti Di Sicurezza Relativi Ai Depositi Di Liquidi Facilmente Infiammabili e/o Tossici. Official Journal of Italian Republic (Gazzetta Ufficiale), Rome (I).

Franke, J., Hellsten, A., Schlunzen, K.H., Carissimo, B., 2011. The COST 732 best practice guideline for CFD simulation of flows in the urban environment: a summary. Int. J. Environ. Pollut. 44, 419. https://doi.org/10.1504/IJEP.2011.038443.

Gant, S.E., Atkinson, G.T., 2011. Dispersion of the vapour cloud in the Buncefield incident. Process Saf. Environ. Prot. 89, 391–403. https://doi.org/10.1016/j.psep.2011.06.018.

Ginestet, S., Le Bot, C., 2018. Evaporation flow assessment from petroleum product storage tanks exposed to fire conditions. Oil & Gas Science and Technology – Revue d'IFP Energies nouvelles 73, 27. https://doi.org/10.2516/ogst/2018023.

HSG176, 2015. Health and Safety Executive (HSE): the Storage of Flammable Liquids in Tanks.

Huang, W., Wang, S., Jing, H., Wang, C., Sun, X., Zhou, N., Fang, J., Fu, L., 2020a. A calculation method for simulation and evaluation of oil vapor diffusion and breathing loss in a dome roof tank subjected to the solar radiation. J. Pet. Sci. Eng. 195, 107568. https://doi.org/10.1016/j.petrol.2020.107568.

Huang, W., Xu, M., Li, F., Ji, H., Fang, J., 2020b. Influence of wind deviation angle on n-Hexane evaporation loss of internal floating-roof tanks. China Pet. Process. Petrochem. Technol. 2.

Luan, X., Zhang, M., Zhao, S., Zhang, B., 2023. Numerical study on the effects of bund on liquid pool spreading and vapor dispersion after a catastrophic LNG tank failure. Process Saf. Environ. Prot. 176, 74–86. https://doi.org/10.1016/j.psep.2023.06.006.

Luketa-Hanlin, A., Koopman, R.P., Ermak, D.L., 2007. On the application of computational fluid dynamics codes for liquefied natural gas dispersion. J. Hazard. Mater. 140, 504–517. https://doi.org/10.1016/j.jhazmat.2006.10.023.

Marsegan, C., Busini, V., Rota, R., 2016. Influence of active mitigation barriers on LNG dispersion. J. Loss Prev. Process. Ind. 44, 380–389. https://doi.org/10.1016/j.jlp.2016.10.010.

Nair, S.R., 2008. Methods of avoiding tank bund overtopping using computational fluid dynamics tool. Inst. Chem. Eng. Symp. Ser. 154.

National Fire Protection Association, 2024. NFPA 30 - Flammable and Combustible Liquids Code (USA).

Persson, H., Lönnermark, A., 2004. Tank Fires: Review of Fire Incidents 1951–2003. SP REPORT 2004:14.

Sotoodeh, K., 2024. A case study demonstrating the use of layers of protection analysis (LOPA) in order to prevent fire and explosion in storage tanks due to overfilling. Safety in Extreme Environments 6, 161–172. https://doi.org/10.1007/s42797-023-00095-3.

Wang, J., Wang, M., Yu, X., Zong, R., Lu, S., 2022. Experimental and numerical study of the fire behavior of a tank with oil leaking and burning. Process Saf. Environ. Prot. 159, 1203–1214. https://doi.org/10.1016/j.psep.2022.01.047.

Zhao, S., Huo, J., Xu, R., Liu, Y., Jing, M., Zhang, B., 2022. Prevention of bund overtopping after a catastrophic tank failure accident: effects of bund design, liquids and scale-up. Process Saf. Environ. Prot. 166, 41–56. https://doi.org/10.1016/j.psep.2022.07.062.